Depletion Kinetics of Nickel Atoms by Sulfur Dioxide

Roy E. McClean

Chemistry Department, United States Naval Academy, Annapolis, Maryland 21402

Received: September 3, 1998; In Final Form: October 22, 1998

The gas-phase depletion kinetics of Ni(a^3F_J, a^3D_J) in the presence of SO_2 are reported. Nickel atoms were produced by the 248 nm photodissociation of nickelocene and detected by laser-induced fluorescence. The ground term of Ni, a^3F_4, and the two lowest energy spin−orbit states, a^3D_3 and a^3D_2, were found to react termolecularly (and with identical rate constants) with SO_2, an indication of rapid interconversion between these states. The limiting low-pressure third-order rate constant, measured over the temperature range 296−612 K, can be expressed as $k_o(T) = 7.455 - 24.41(\log T) + 3.993(\log T)^2$ cm^6 molecule^{-2} s^{-1}. A binding energy of 47 kcal mol^{-1} was estimated by combining the kinetic results with unimolecular rate theory and density functional methods. The limiting high-pressure second-order rate constant over the temperature range is on the order of the collision rate. The other spin−orbit states of both terms depleted quite rapidly in the presence of SO_2, with rate constants also on the order of the collision rate.

Introduction

There have been several recent investigations of bimolecular reactions of transition-metal (TM) atoms with SO_2.[1−5] These reactions are of interest, in part, because of the importance of SO_2 in acid rain and in the corrosion of metals. Many of the gas-phase reactions have been observed to proceed with little or no barriers. In most cases, the relatively fast rates have been attributed to an electron-transfer mechanism whereby an electron is transferred from the TM atom to the SO_2. Due to the relatively large ionization energies of TM atoms, valence interactions are expected to play a role in their reactions; i.e., the reactions are driven not only by an electron transfer, but also by the type of orbital occupancies of the TM atoms.

In this paper, the depletion of Ni(a^3F_J, a^3D_J) by SO_2 is reported. Unlike the previous work on TM + SO_2 reactions where abstraction mechanisms were indicated, an abstraction reaction is not thermodynamically feasible for the ground state of Ni. The Ni + SO_2 reaction is endothermic at relatively low temperatures[6,7] and, therefore, a termolecular mechanism is the only viable reaction channel at room temperature. This work provides information on the efficiency of 1:1 adduct formation between Ni and SO_2. It also allows one to determine if the Ni excited states deplete at appreciable rates in the presence of SO_2, as observed in other TM + SO_2 systems. Density functional theory (DFT)[8] and Troe's factorization method[9] are combined with the kinetic results to estimate the binding energy of the $NiSO_2$ adduct.

Experimental Section

Details of the experimental arrangement have been described in detail elsewhere[10] and are only summarized here. The laser-photolysis/laser-induced fluorescence (LP/LIF), slow-flow technique was used in this work. The reaction chamber was a stainless steel cross with gas inlet and outlet ports, a viewport for LIF detection, and windows for passage of the laser beams; the chamber was contained in a convection oven capable of attaining temperatures up to 628 K. Nickelocene, the nickel precursor, was entrained in a flow of argon gas. The buffer gas (argon), diluted precursor, and SO_2 passed through separate mass flow controllers after which they combined into one line and entered the reaction chamber. A slow flow of argon passed over the windows in order to minimize the deposition of the precursor and photofragments. Total flows were between 150 and 8500 sccm, depending on the total pressure. Partial pressures of the individual components were determined by their relative flows and the total pressure in the reaction chamber. Pressures were measured by Baratron manometers, and temperatures were measured with a thermocouple attached to the reaction chamber.

TABLE 1: Atomic States of Ni and LIF Information[a]

Ni state[b]	energy (cm^{-1})	λ (nm) of excitation[c]
a^3F_4	0	343.728
a^3F_3	1332.153	346.750
a^3F_2	2216.519	348.377
a^3D_3	204.786	341.476
a^3D_2	879.813	349.296
a^3D_1	1713.080	345.846

[a] The detection filter was centered at 350 nm and had fwhm = 10 nm. [b] Reference 11. [c] Reference 12.

Nickel atoms were produced from $Ni(C_5H_5)_2$ by the unfocused output of an excimer laser operating on KrF (248 nm) at 21 Hz. Rate-constant measurements did not depend on the photolysis fluences, which were approximately 200−400 mJ cm^{-2} in the reaction chamber. Detection of nickel atoms was by LIF using laser light from an excimer-pumped dye module. The photolysis and dye beams counterpropagated through the chamber. Neutral density filters were used to ensure that the dye laser fluence (less than 1 mJ/pulse) did not affect the kinetic results. The Ni states studied and the corresponding excitation wavelengths are listed in Table 1.[11,12] A photomultiplier tube and lens focusing system, situated 90° to the laser beams, collected the LIF signal, which was subsequently sent to a gated boxcar sampling module, and the boxcar's output was stored and analyzed by a computer.

All kinetic results are based on the disappearance of Ni atoms under pseudo-first-order conditions, where the number density of Ni was much less than the number density of SO_2 and Ar. Reaction time was taken as the delay time between the laser

10.1021/jp983594p CCC: $18.00
Published on Web 12/10/1998

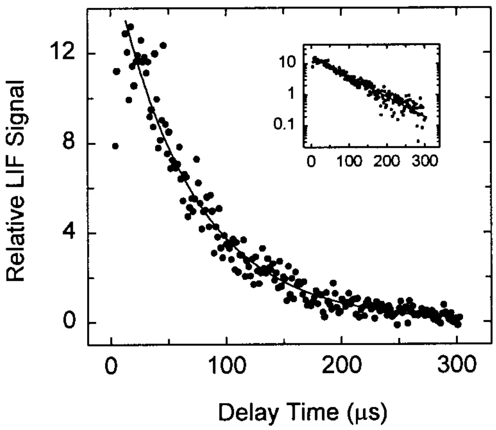

Figure 1. Typical decay profile of Ni in the presence of SO_2. Data are for Ni(a^3D_3.). T = 296 K, P_{tot} = 40 Torr, P_{SO_2} = 16.8 mTorr. The solid line through the data is an exponential fit with τ = 68.0 μs. The inset is the same data in semilogarithmic form; note the linearity.

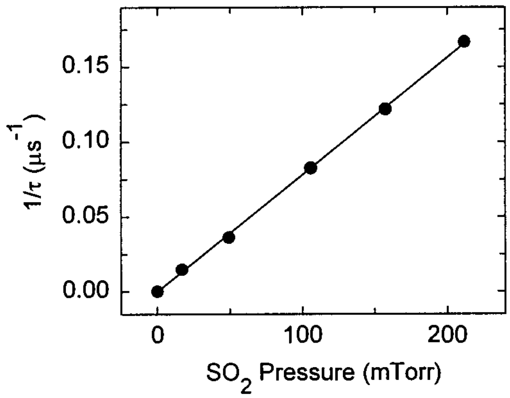

Figure 2. Typical plot for determining second-order rate constants. The conditions are the same as in Figure 1, except the partial pressures of SO_2 are changing. Each point represents an average of 2−3 measurements. The slope gives k = (2.40 ± 0.06) × 10^{-11} cm^3 molecule^{-1} s^{-1}, where the uncertainty is $\pm 2\sigma$ from the linear regression.

pulses. For a given experimental run, the delay time was varied by a digital delay generator controlled by a computer. Minimum delay times were typically 1−10 μs in order to prevent overlap of the prompt emission with the LIF signal. The trigger source for these experiments was scattered pump laser light incident upon a fast photodiode. LIF decay traces consisted of 200−500 points, each point averaged over 2−10 laser shots. LIF intensities were proportional to Ni number densities.

Reagents. The following reagents were used as received: Ni(C_5H_5)$_2$ (Strem Chemicals, Inc., 99%), Ar (Potomac Airgas, Inc., 99.998%), SO_2 (MG Industries, 99.98%).

Data Analysis and Results

A typical decay trace is shown in Figure 1. It represents the decay of Ni(a^3D_3) in the presence of added SO_2. Partial pressures of the precursor nickelocene are not accurately known in these experiments. However, based on the carrier flow rate and pressure, total flow rate, and total pressure, nickelocene's partial pressure in the reaction chamber is estimated to be less than 0.5 mTorr for all experiments. The solid line through the data is an exponential fit to the equation

$$I = I_o \exp(-t/\tau) \tag{1}$$

where I and I_o are the LIF signals at time t and time t = 0, respectively, and τ is the lifetime from which the pseudo-first-order rate constant, $1/\tau$, is obtained. $1/\tau$ is given by

$$1/\tau = 1/\tau_o + k[SO_2] \tag{2}$$

where τ_o is the lifetime of Ni without added SO_2, k is the second-order rate constant, and [SO_2] is the partial pressure of SO_2. τ_o represents the lifetime of Ni in the presence of species other than SO_2 in the reaction chamber and diffusion out of the detection zone. τ_o was usually long compared to τ. Second-order rate constants were obtained from the slopes of plots of $1/\tau$ vs SO_2 partial pressure such as that shown in Figure 2. Note that the intercept ($1/\tau_o$) is relatively small so that interference from photofragments and diffusion was minimal.

The measured rate constants are listed in Table 2. The uncertainties resulting from the linear regression fits, such as that in Figure 2, were approximately 3% ($\pm 1\sigma$) in precision. The overall uncertainties, estimated at ±30% at the 95% confidence limit, include statistical scatter in the data, the

TABLE 2: Measured Second-Order Rate Constants for the Depletion of Ni (a^3F_J, a^3D_J) by SO_2[a]

		k (10^{-11} cm^3 molecule^{-1} s^{-1})				
state	P (Torr)	296 K	349 K	399 K	498 K	612 K
a^3F_4	10	0.760				
	20	1.39		0.494		
	120	4.83		2.41		
a^3F_3	10	17.9				
a^3F_2	10	15.5				
a^3D_3	10	0.799	0.416	0.299	0.138	
	20	1.49	0.718	0.489	0.243	0.107
	40	2.40	1.17	0.891	0.399	0.176
	80	3.82	2.38	1.52	0.792	0.336
	120	4.63	3.21	2.07	1.10	0.476
	200	5.79	4.07	2.83	1.70	0.737
	300	6.79	5.54	3.89	2.18	1.06
	400	8.27	6.01	4.59	3.10	1.41
	500	8.97	7.33	5.16	3.19	1.52
	600	9.32	7.51	5.85	4.01	1.95
a^3D_2	10	0.793				
	40	2.19				
a^3D_1	10	13.2				

[a] Buffer = argon. Overall uncertainties are ±30% at the 95% confidence limit.

reproducibility of k, and instrumental uncertainties such as digital delay and flow measurements. The rate constants for the depletion of the a^3F_4, a^3D_3, and a^3D_2 states are identical. These rate constants increase with increasing total pressure and decrease with increasing temperature, an indication of the termolecular reaction mechanism

$$\mathrm{Ni} + \mathrm{SO_2} \rightleftharpoons \mathrm{Ni{-}SO_2}^* \tag{3}$$

$$\mathrm{Ni{-}SO_2}^* + \mathrm{M} \rightarrow \mathrm{Ni{-}SO_2} + \mathrm{M} \tag{4}$$

The third body M was predominantly argon. The partial pressures of the other gaseous components were too low to contribute significantly to the stabilization of the $NiSO_2^*$ adduct. Data were not collected above 600 Torr and 612 K because of a low signal-to-noise ratio under such conditions. Since the depletion rate constants of the a^3F_4, a^3D_3, and a^3D_2 states are identical, a thorough pressure and temperature-dependence study was undertaken for only Ni(a^3D_3), because it had the largest LIF signal.

Plots of the second-order rate constants (for a^3D_3) as a function of total pressure at all temperatures are shown in Figures 3 and 4. The lack of any true bimolecular component

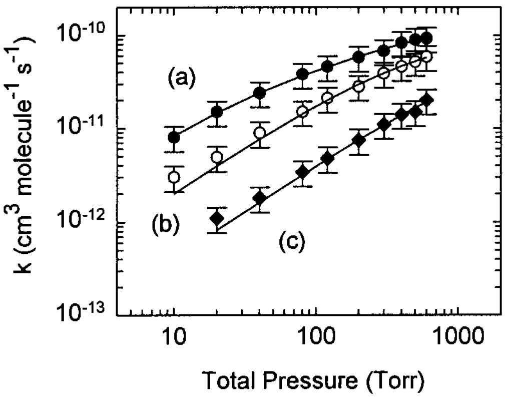

Figure 3. Pressure dependence of $Ni(a^3D_3) + SO_2$ at (a) 296, (b) 399, and (c) 612 K. The solid line through the data at 296 is a fit to eq 6, and the solid lines through the other data are fits to eq 7. See Table 3 for results of fits.

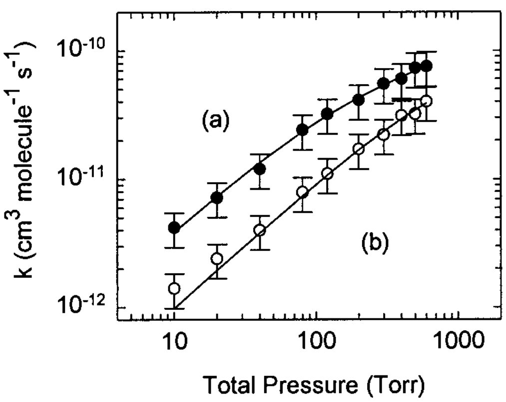

Figure 4. Pressure dependence of $Ni(a^3D_3) + SO_2$ at (a) 349 and (b) 499 K. The solid lines through curves (a) and (b) are fits to eqs 6 (with fixed k_∞) and 7, respectively. See Table 3 for results of fit.

to the rate is consistent with the thermochemistry of the ground state, bimolecular channel

$$\mathrm{Ni} + \mathrm{SO_2} \rightarrow \mathrm{NiO} + \mathrm{SO} \qquad \Delta H \approx 40\ \mathrm{kcal\ mol^{-1}}\ {}^{6,7} \quad (5)$$

being thermodynamically inaccessible at relatively low temperatures. The solid line through the 296 data is a fit using Troe's formalism[9]

$$\log k = \log \frac{k_o[M]}{1 + (k_o[M]/k_\infty)} + \frac{\log F_c}{1 + [\log (k_o[M]/k_\infty)]^2} \quad (6)$$

where k_o is the limiting low-pressure third-order rate constant, k_∞ is the limiting high-pressure second-order rate constant, $[M]$ is the buffer gas number density, and F_c is the broadening factor. Large uncertainties (>100%) in the fitted parameters were obtained when the higher temperature data were fitted to eq 6. Thus, for the 349 K data, k_∞ was fixed at 1.5×10^{-10} cm^3 molecule^{-1} s^{-1} in eq 6. The simplified Lindemann–Hinshelwood expression[13]

$$k = k_o [M]/(1 + k_o[M]/k_\infty) \quad (7)$$

was used for the higher temperature data. Results of the fits are given in Table 3. k_o decreases with increasing temperature, as shown in Figure 5, and can be expressed as

$$k_o(T) = 7.455 - 24.41(\log T) + 3.993(\log T)^2\ \mathrm{cm^6\ molecule^{-2}\ s^{-1}} \quad (8)$$

TABLE 3: Falloff Modeling Parameters for the Reaction of Ni ($a^6D_{1/2}$, a^4F_J) with SO_2

T (K)	k_o (cm^6 molecule^{-2} s^{-1})	k_∞ (cm^3 molecule^{-1} s^{-1})	F_c
296	$(3.3 \pm 0.3) \times 10^{-29}$	$(1.7 \pm 0.4) \times 10^{-10}$	0.64 ± 0.10
349	$(1.6 \pm 0.2) \times 10^{-29}$	1.5×10^{-10} (fix)	0.79 ± 0.07
399	$(0.84 \pm 0.08) \times 10^{-29}$	$(1.1 \pm 0.2) \times 10^{-10}$	*a*
498	$(0.51 \pm 0.08) \times 10^{-29}$	$(1.1 \pm 0.5) \times 10^{-10}$	*a*
612	$(0.26 \pm 0.05) \times 10^{-29}$	$(0.84 \pm 0.47) \times 10^{-10}$	*a*

[a] The simplified Lindemann–Hinshelwood mechanism, eq 7, was used to fit the data. The uncertainties represent two standard deviations (precision).

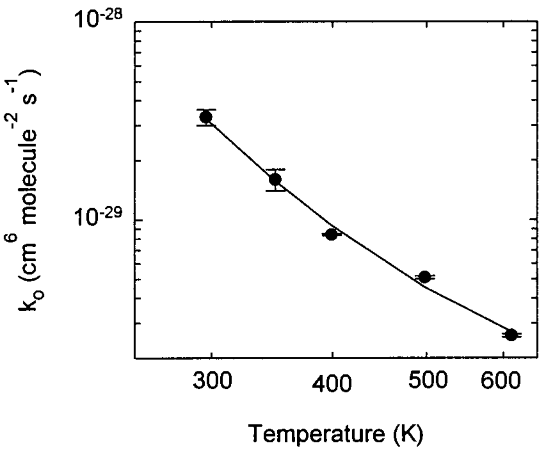

Figure 5. Temperature dependence of k_o. The solid line through the data is a polynomial fit. See text for results of fit. The error bars represent the $\pm 2\sigma$ uncertainties (precision).

k_∞ appears to decrease with increasing temperature. However, the relatively long extrapolations of the second-order rate constants to the high-pressure limit as the temperature increases and the combined uncertainties in k_∞ precluded an accurate assessment of this observation. The k_∞ values obtained from eqs 6 and 7 are on the order of the gas kinetic rate constant of $\sim 2 \times 10^{-10}$ cm^3 molecule^{-1} s^{-1}, thus justifying the use of $k_\infty = 1.5 \times 10^{-10}$ cm^3 molecule^{-1} s^{-1} for the 349 K data.

Table 2 shows that the excited states above 880 cm^{-1} deplete at approximately the gas collision rate, an indication of no activation barrier. The kinetics of these states were not investigated at total pressures above 10 Torr due to decreasing signal-to-noise ratios. A pressure dependence and a positive temperature dependence are not expected since the depletion rate constants are large.

Discussion

The results presented here indicate that the excited states below 880 cm^{-1} deplete at identical rates and/or the rate of interconversion among them is fast. The thermal energy is 206 cm^{-1} and the a^3D_3 state is only 205 cm^{-1} above the ground state. Thus, rapid interconversion is likely, at least between the a^3F_4 and a^3D_3 states. ($Ni(a^3D_3)$ and $Ni(a^3D_2)$ account for approximately 22% and 3%, respectively, of the thermal population at 296 K.) $Ni(a^3F_4)$, $Ni(a^3D_3)$, and $Ni(a^3D_2)$ were also found to react with NO at identical rates at ~1 Torr total pressure, and none of these states reacted with O_2 and N_2O.[14] Rapid interconversion between the states was not indicated in that work. It thus appears that the depletion mechanism of Ni(a^3D_2) in the presence of small oxidants is similar to that of $Ni(a^3F_4)$ and $Ni(a^3D_3)$. The $3d^84s^2$ electron configuration of the ground state does not appear to introduce any barriers to reaction. Since the a^3F_4 state is in thermal equilibrium with the

$3d^94s^1$ a^3D_3 state, any barriers due to the closed s-subshell could be screened. On the basis of the orbital-occupancy argument presented above, we conclude that the ground state is converted to the a^3D_3 state, which is reactive. k_∞ is close to the gas kinetic rate constant, and k_o decreases with increasing temperature, indications of no energy barrier to product formation.

Physical quenching is the likely depletion channel of the states above 880 cm^{-1}. An abstraction channel is not accessible, and rate constants on the order of 10^{-10} cm^3 s^{-1} for a termolecular channel at only 10 Torr total pressure is not expected. *E*−*V* energy transfer may take place via the vibrational modes of SO_2 since the energy differences between the Ni states are close to the vibrational modes of SO_2.[7]

To *estimate* the binding energy E_b of the $NiSO_2$ adduct relative to Ni(a^3D_3), simplified RRKM calculations using the formalism of Troe[9] were performed at 296 K. In brief, the rate constant for the unimolecular dissociation in the low-pressure limit, k_{uni}, of $NiSO_2$ was first calculated. k_o was then calculated from the equilibrium expression $K_{eq} = k_{uni}/k_o$, where K_{eq} is the equilibrium constant for $NiSO_2 \rightleftharpoons Ni + SO_2$. The collision efficiency, β_c, of Ar was assumed to be 0.20. β_c can be determined by comparing the experimental and calculated (strong collision) third-order rate constants. However, the uncertainties and adjustable binding energy in the calculations precluded such an approach. The molecular structure and vibrational frequencies of $NiSO_2$ needed for the RRKM calculations were calculated from density functional[8] methods. The binding energy was varied until agreement was obtained between the calculated and experimental third-order rate constant. The density functional calculations are not intended to be exhaustive, but instead serve mainly to provide estimates of the molecular parameters.

The molecular parameters of $NiSO_2$ were calculated by the SPARTAN[15,16] suite of programs. Calculations were performed with the LSDA/pBP86 model and DN** numerical basis sets. Several triplet isomers were assumed. The “side-on bonded,” $\eta^2_{O,O}$ isomer (C_{2v} geometry) gave the lowest energy. The DFT results are to be taken with caution; numerical errors are likely since calculations involve numerical integration steps. Additionally, the relatively large number of low-lying states of Ni and other TM atoms poses a challenge for the theoretical treatment of transition metals. Pertinent output from the computations are listed in the Appendix.

Agreement between the measured and calculated k_o at 296 K was obtained for $E_b = 47 \pm 3$ kcal mol^{-1}; the uncertainty in E_b is based only on the overall uncertainty in k_o at 296 K. Since there is no activation barrier, significantly smaller E_b values would give association rate constants that are too small because k_o is a sensitive function of the binding energy.[13] The presence of several low-lying states in atomic Ni and the possibility of several low-lying bound states in $NiSO_2$ could lead to additional pathways, thus affecting the calculated results. The equilibrium constant, and hence k_o, is also affected by the relatively low level of the DFT calculations. Thus, only an estimate of E_b is reported. This estimate is reasonable, however. A comparison of the rates of TM and main-group metals with small oxygen-containing molecules indicates that a bond energy of 40−50 kcal mol^{-1} is in accord with third-order rate constants of the magnitude measured in this work.[17−21]

The binding energies of Na−SO_2 and K−SO_2 have been found to lie within the range of the corresponding binding energies of the metal−O_2 superoxides.[19,20] C_{2v} $\eta^2_{O,O}$-type structures, where the alkali-metal atoms are side-bonded to the oxygen atoms, are observed and calculated. The binding energy of $NiSO_2$ estimated in this work is approximately equal to the binding energy of C_{2v} $\eta^2_{O,O}$ Ni−O_2 from an ab initio study: $E_b = 48 \pm 7$ kcal mol^{-1}.[22] This observation suggests that the bonding in C_{2v} NiO_2 and C_{2v} $NiSO_2$ is similar. Covalent and ionic components are present in NiO_2. The relatively large limiting low-pressure and high-pressure rate constants for Ni + SO_2 and the larger electron affinity of SO_2 (than O_2)[6] suggest an ionic component in $NiSO_2$.

The reaction of Mn($3d^54s^2$ $a^6S_{5/2}$) with SO_2 was also investigated in this work to determine if a relatively unreactive TM atom would react with SO_2. An upper limit of $\sim 10^{-14}$ cm^3 $molecule^{-1}$ s^{-1} was obtained over the temperature range of 296−622 K. The electron-transfer mechanism has been offered as an explanation for the reactions of TM atoms with SO_2. The ionization energy of Mn is less than that of Ni.[6] Thus, the orbital occupancy of the TM atom is the predominant driving force (at least when comparing Mn and Ni).

Summary and Conclusions

Results presented here indicate that Ni is very reactive toward SO_2. The three lowest states of Ni, a^3F_4, a^3D_3, and a^3D_2, react with SO_2 via a termolecular mechanism. The 1:1 adduct formation is efficient. The kinetic results were combined with DFT and RRKM calculations to provide an *estimate* of 47 kcal mol^{-1} for the binding energy of $NiSO_2$ ($\eta^2_{O,O}$ isomer). A comparison between NiO_2 and $NiSO_2$ suggest covalent and ionic components to the bonding in $NiSO_2$. The a^3F_3, a^3F_2, and a^3D_1 states of Ni deplete at approximately the gas collision rate in the presence of SO_2.

Acknowledgment. This research was supported by the Naval Academy Research Council and a Cottrell College Science Award of Research Corporation.

Appendix

The DFT suite of SPARTAN programs[15,16] was used to calculate the molecular parameters of $NiSO_2$. For the triplet $\eta^2_{O,O}$ isomer of $NiSO_2$ (C_{2v} geometry), we found bond lengths of r(S−O) = 1.5847 Å and r(O−Ni) = 1.9539 Å. Bond angles are ∠(O−S−O) = 100.1412°, ∠(S−O−Ni) = 91.4730°, and ∠(O−Ni−O) = 76.9128°. Calculated frequencies, in units of cm^{-1}, are 127.12, 301.61, 349.38, 504.62, 836.33, and 841.61.

For the simplified RRKM calculations at 296 K, E_o was taken as an adjustable parameter. The rate constant for the unimolecular dissociation in the low-pressure limit, k_{uni}, is given by [9]

$$k_{uni} = \beta_C Z_{LJ} \frac{\rho(E_o)RT}{Q_{vib}} \exp(-E_o/RT) F_{anh} F_E F_{rot} F_{rotintn} F_{corr}$$

where β_C is the collisional efficiency of Ar, Z_{LJ} is the Leonard−Jones rate constant, $\rho(E_o)$ is the vibrational density of states of $NiSO_2$ at the threshold energy E_o for dissociation, Q_{vib} is the vibrational partition function of $NiSO_2$, F_{anh} is a correction for vibrational anharmonicity, F_E is a correction for the variation of the density of states, and F_{rot} is the molecular rotational correction factor. The corrections for internal rotational modes and the coupling of the F factors, $F_{rot\ int}$ and F_{corr}, were taken as one.

A Lennard−Jones collision frequency of 6.38×10^{-10} cm^3 $molecule^{-1}$ s^{-1} was calculated from reasonable values of the Lennard−Jones parameters. β_c was taken as 0.20. $s = 6$ and $m = 3$, where s is the number of vibrational modes in $NiSO_2$ and *m* is the number of vibrational modes that has disappeared after dissociation. $E_o = 47$ kcal mol^{-1}. Calculated RRKM parameters are $a(E_o) = 0.989$, $F_{anh} = 1.37$, $F_E = 1.06$, and $F_{rot} = 22.4$, where $a(E_o)$ is a constant calculated from the energy. Calculated K_{eq}, k_{uni}, and k_o values are 3.14×10^{-10} molecule cm^{-3}, 5.17×10^{-38} cm^3 molecule^{-1} s^{-1}, and 3.30×10^{-29} cm^6 molecule^{-2} s^{-1}, respectively.

References and Notes

(1) McClean, R. E.; Campbell, M. L.; Kolsch, E. J. *J. Phys. Chem. A* **1997**, *101*, 3348.

(2) Campbell, M. L.; Hooper, K. L.; Kolsch, E. J. *Chem Phys. Lett.* **1997**, *274*, 7.

(3) McClean, R. E.; Campbell, M. L.; Goodwin, R. H. *J. Phys. Chem.* **1996**, *100*, 7502.

(4) Harter, J. S. S.; Campbell, M. L.; McClean, R. E. *Int. J. Chem. Kinet.* **1997**, *29*, 367.

(5) Campbell, M. L.; McClean, R. E. *J. Phys. Chem.* **1993**, *97*, 7942.

(6) *CRC Handbook of Chemistry and Physics*, 75th ed.; Lide, D. R., Ed.; CRC Press: Boca Raton, FL, 1995.

(7) JANAF Thermochemical Tables, 3rd ed. *J. Phys. Chem. Ref. Data* Chase, M. W., Jr., Davies, C. A., Downey, J. R., Jr., Frurip, D. J., McDonald, R. A., Syverud, A. N., Eds.; **1985**, *14*, Suppl. 1.

(8) *Modern Density Functional Theory: A Tool for Chemistry*; Seminario, J. M., Politzer, P., Eds.; Elsevier: New York, 1995.

(9) Troe, J. *J. Phys. Chem.* **1979**, *83*, 114.

(10) Campbell, M. L.; McClean, R. E. *J. Chem. Soc., Faraday Trans.* **1995**, *91*, 3787.

(11) Moore, C. E. Atomic Energy Levels as Derived from the Analysis of Optical Spectra. *Natl. Stand. Ref. Data Ser.* (*U.S. Natl. Bur. Stand.*) **1971**, NSRDS-NBS 35.

(12) Martin, G. A.; Fuhr, J. R.; Wiese, W. L. *J. Phys. Chem. Ref. Data* **1988**, *17*, Suppl. 4.

(13) Gilbert, R. G.; Smith, S. C. *Theory of Unimolecular and Recombination Reactions*; Blackwell Scientific Publications: Boston, 1990.

(14) Matsui, R.; Senba, K.; Honma, K. *J. Phys. Chem. A* **1997**, *101*, 179.

(15) *SPARTAN*; Wavefunction, Inc.: Irvine, CA, 1997.

(16) Hedre, W. J.; Lou, L. *A Guide to Density Functional Calculations in SPARTAN*; Wavefunction, Inc.: Irvine, CA, 1997.

(17) Brown, C. E.; Mitchell, S. A.; Hackett, P. A. *J. Phys. Chem.* **1991**, *95*, 1062 and references therein.

(18) Parnis, J. M.; Mitchell, S. A.; Hackett, P. A. *J. Phys. Chem.* **1990**, *94*, 8152 and references therein.

(19) Goumri, A.; Laakso, D.; Rocha, J.-D. R.; Francis, E.; Marshall, P. *J. Phys. Chem.* **1993**, *97*, 5297.

(20) Shi, Y.; Marshall, P. *J. Phys. Chem.* **1991**, *95*, 1654.

(21) Nien, C.-F.; Rajasekhar, B.; Plane, J. M. C. *J. Phys. Chem.* **1993**, *97*, 6449.

(22) The binding energy of 48 ± 7 kcal mol^{-1} was obtained from Bauschlicher, C. W., Jr.; Langhoff, S. R.; Partridge, H.; Sodupe, M. *J. Phys. Chem.* **1993**, *97*, 856. A kinetic study of Ni + O_2 yielded a binding energy of 57 kcal mol^{-1} (ref 23), and a previous theoretical study yielded a value of 18 kcal mol^{-1} (ref 24).

(23) Mitchell, S. A. In *Gas-Phase Metal Reactions*; Fontijn, A., Ed.; Elsevier: Amsterdam, 1992; p 227.

(24) Blomberg, M. R. A.; Siegbahn, P. E. M.; Strich, A. *Chem. Phys.* **1985**, *97*, 287.